Since January 2020 Elsevier has created a COVID-19 resource centre with free information in English and Mandarin on the novel coronavirus COVID-19. The COVID-19 resource centre is hosted on Elsevier Connect, the company's public news and information website.

Journal of Molecular Structure 1225 (2021) 129230

Contents lists available at ScienceDirect

Journal of Molecular Structure

journal homepage: www.elsevier.com/locate/molstr

Synthesis, characterization and computational study on potential inhibitory action of novel azo imidazole derivatives against COVID-19 main protease (M^{pro}: 6LU7)

Abhijit Chhetri[a], Sailesh Chettri[b], Pranesh Rai[c], Dipu Kumar Mishra[c], Biswajit Sinha[c], Dhiraj Brahman[b,*]

[a] Department of Microbiology, St. Joseph's College, Darjeeling-734104, India
[b] Department of Chemistry, St. Joseph's College, Darjeeling-734104, India
[c] Department of Chemistry, University of North Bengal, Darjeeling-734013, India

ARTICLE INFO

Article history:
Received 12 July 2020
Revised 8 September 2020
Accepted 8 September 2020
Available online 18 September 2020

Keywords:
ADME
Azo imidazole
Molecular docking
Sars-cov-2
Pharmacokinetics
6lu7

ABSTRACT

A series of six novel imidazole anchored azo-imidazole derivatives (L1-L6) have been prepared by the simple condensation reaction of azo-coupled ortho-vaniline precursor with amino functionalised imidazole derivative and the synthesized derivatives (L1-L6) have been characterized by different analytical and spectroscopic techniques. Molecular docking studies were carried out to ascertain the inhibitory action of studied ligands (L1-L6) against the Main Protease (6LU7) of novel coronavirus (COVID-19). The result of the docking of L1-L6 showed a significant inhibitory action against the Main protease (M^{pro}) of SARS-CoV-2 and the binding energy (ΔG) values of the ligands (L1-L6) against the protein 6LU7 have found to be -7.7 Kcal/mole (L1), -7.4 Kcal/mole (L2), -6.7 Kcal/mole (L3), -7.9 Kcal/mole (L4), -8.1 Kcal/mole (L5) and -7.9 Kcal/mole (L6). Pharmacokinetic properties (ADME) of the ligands (L1-L6) have also been studied.

1. Introduction

Severe Acute Respiratory Syndrome-2 (SARS-CoV-2) or COVID-19, a novel pathogen belonging to a class of large and diverse family of enveloped, positive RNA viruses outbreak in Wuhan city of China in late December 2019 and by the beginning of the year 2020, it has became one of the most debilitating and lethal viral respiratory disease which attack the respiratory tract, causing difficulties in breathing, cough, high fever, sore throat, diarrhea, effects gastrointestinal system, heart, kidney and central nervous system leading to multiple organ failure and ultimately even death as similar to the infection caused by SARS-CoV and MERS-CoV [1–3]. By the end of February 2020 and beginning of the March 2020, the SARS-CoV-2 infection disease spread almost in every country around the world and World Health Organization (WHO) on March 11th 2020 declared SARS-CoV-2 disease as pandemic [4]. As of June 17th 2020, more than 8.4 million people were infected and nearly 0.45 million people have succumbed to the SARS-CoV-2 epidemic (worldometer, June 17th 2020). Recent studies on SARS-CoV-2 have shown that the genome of SARS-CoV-2 is over 80% similar to previously reported SARS-CoV and spike protein receptor binding domain (RBD) and its host receptor (ACE2) similar to that of SARS-CoV is mainly responsible for cross species and human to human transmission of SARS-CoV-2 virus [5–8]. As of now, no potential and specific therapeutic agents or vaccine is approved or available [9]. Many researchers and scientists around the world are engaged in developing specific and potential antiviral drug or vaccine to treat the SARS-CoV-2 infection [10–11]. However, only a supportive measures in terms of FDA approved antiviral, antimalarila drugs and therapeutic agents such as remdesivir, hydroxychloroquine, chloroquine, lopinavir, umifenovir, favipiravir, and oseltamivir and Ascorbic acid, Azithromycin, Corticosteroids, Nitric oxide, IL-6 antagonists as a clinical management are available for the treatment of SARS-CoV-2 disease till date [12]. Many research studies on viruses such as HIV virus, Hepatitis C virus and Ebola virus have shown that the viral protease is the common target for the development of antiviral drugs [13–15]. Since, the main protease (Mpro) or 3CLPro) of coronavirus is conserved among the coronaviruses and it is mainly responsible for the viral replication [16–17]. Thus, any inhibitors which inhibit the main protease (3CLpro or M^{pro}) and block the replication of SARS-CoV-2 would be effective and specific measures for the development

* Corresponding author.
E-mail address: dhirajslg2@gmail.com (D. Brahman).

https://doi.org/10.1016/j.molstruc.2020.129230
0022-2860/

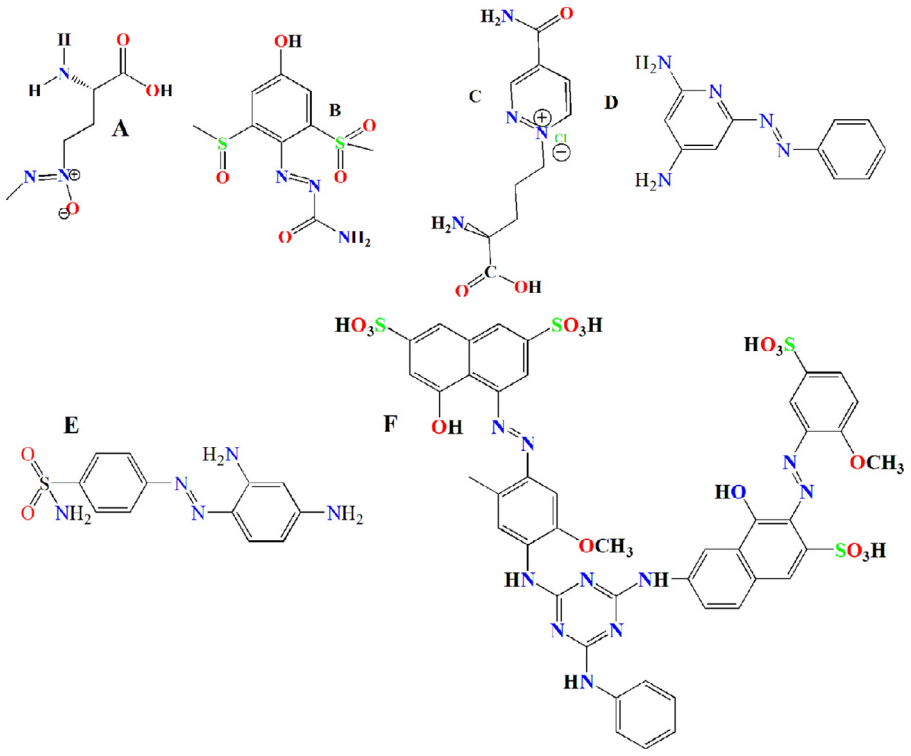

Fig. 1. Chemical structure of some naturally occurring azo alkaloids and FDA approved drugs containing Azo group, A: Azoxybacilin, B: cranformin, C: pyridazomycin, D:: Phenazopyridine, E: Prontosil and F: HIV-1 inhibitor (ADS-J1).

of therapeutic agents or antiviral drugs against SARS-CoV-2 [18]. Again, it is well known that the development and discovery of new therapeutic agents or drugs by traditional methods is time consuming, costly and rigorous scientific *in-vivo* and *in-vitro* processes and therefore, to supplement the old traditional method, now a day, computer aided *in silico* techniques are gaining lot of importance for the designing and formulation of new therapeutic agents or drugs [19–20]. On the other hand, among the various nitrogen containing heterocyclic compounds, imidazole ring are ubiquitous in natural products and possess unique structural features with wide spectrum of biological activities [21]. Thus, unique structural features and electron rich property of imidazole ring have been exploited by pharmaceutical industries for designing, formulating and development of imidazole based therapeutic agents in the wide spectrum of medicinal filed such as anticancer, anti HIV, antimicrobial, anticonvulsant, antihypertensive, analgesic, anti-inflammatory, antidepressant, analgesic, antileishmanial, anticonvulsant, anti-inflammatory etc. [22–24]. Again, natural diazo (-*N* = *N*-) alkaloid compounds are found in many microorganism, marine organisms, plant parts, fungi and ascomycetes and diazo compounds by virtue of possessing diverse biological activities have been used in various fields such as antiviral, antibacterial, antifungal, antitumor, hypotensive and anti-inflammatory therapeutic agents [25–39]. Some of the azo compounds have found to posses excellent inhibitory potential towards HIV-1 protein (Fig. 1) [40]. Moreover, prontosil, an antibacterial drug and phenazopyridine, local analgesic effects on urinary tract infection are FDA approved drugs which contain azo linkage [41–43]. Chemical structures of some naturally occurring azo alkaloid compounds and FDA approved drugs are depicted in Fig. 1.

Thus, incorporation of imidazole ring and diazo ($N = N$) moiety in a single molecule could result in formulation of compounds with interesting properties and diverse biological activities. Therefore, in continuation to our research work in the field of synthesis of azo imidazole derivatives, herein, we report the synthesis of six novel azo imidazole derivatives and an attempt has been made to carry out computational study on inhibitory potential of these novel azo imidazole derivatives against the main protease ((M^{pro}: 6LU7) of SARS-CoV-2.

2. Experimental

2.1. Materials and methods

Analytical grade solvents and reagents (Sd fine chemical company India and Sigma Aldrich) were used without further purification for the synthesis of azo imidazole derivatives. The azo aldehyde precursors and amino functionalized imidazole were prepared by following the literature procedure [44–47]. The IR spectra of the synthesized compounds were measured using Perkin-Elmer Spectrum FT-IR spectrometer (RX-1) in KBr pellets. ^{1}H NMR spectra (chemical shift values are quoted in δ ppm) were recorded at room temperature on Bruker Advance-II NMR Spectrometer operating at 400 MHz magnetic field in DMSO–d_6 solvent with reference to tetramethylsilane (TMS) as an internal standard. Elemental microanalyses (C, H and N) were measured in Perkin–Elmer (Model 240C) analyzer. The purity of the prepared compounds was checked by thin layer chromatography (TLC) on silica gel plates coated in aluminum sheets (silica gel 60 F254).

2.2. Preparation of protein and ligand for docking study

The X-ray crystallographic structure of main protease (M^{por}, PDB ID 6LU7) of SARS-CoV-2 has been downloaded from the Protein Data Bank (PDB) (http://www.pdb.org.) database. Preparation

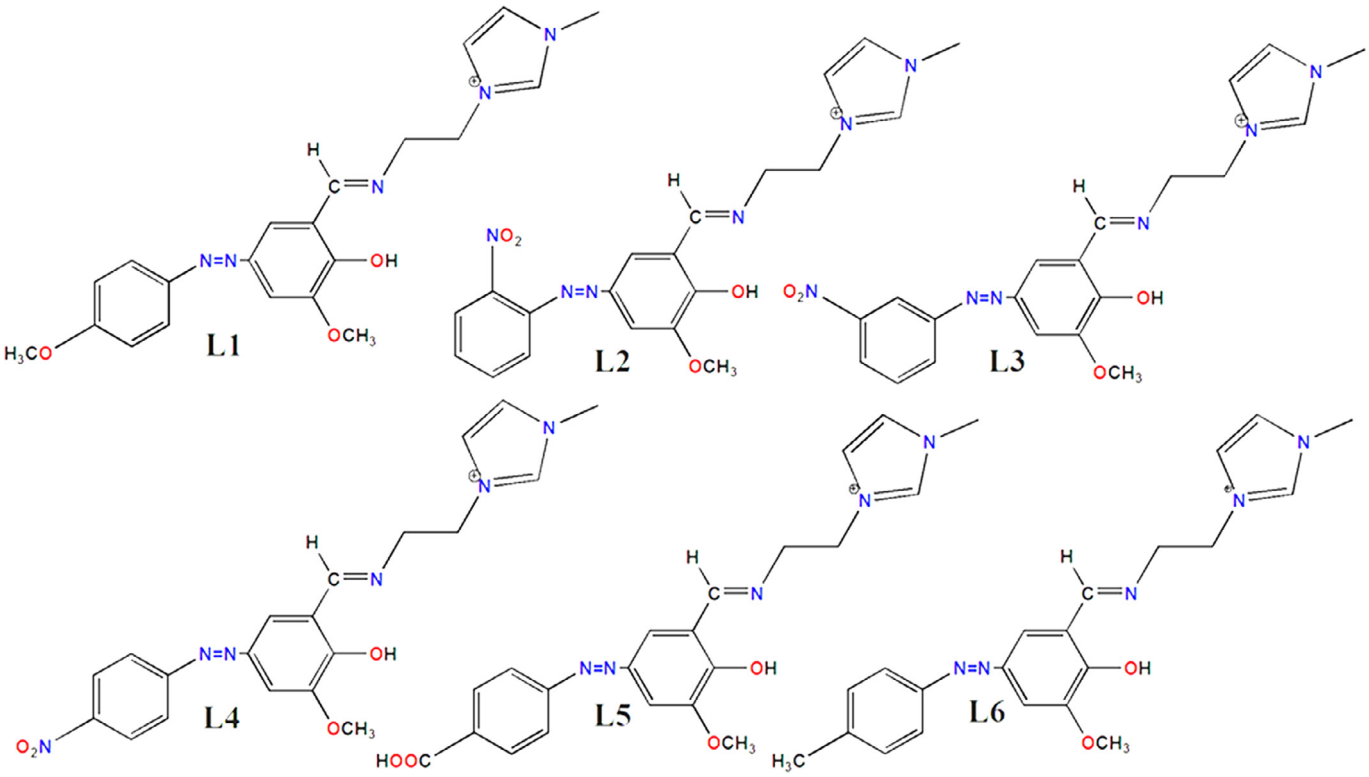

Fig. 2. Structure of Azo Imidazole ligands (L1-L6).

of protein for docking simulation was achieved by using Graphical User Interface program "Auto Dock Tools (ADT) 1.5.6" (Molecular Graphics Laboratory tool or MGL tool) developed by Scripps Research Institute [48]. Specific chain (Chain A) of the protein (6LU7) has been selected for the preparation of receptor protein input file for docking study. Receptor protein preparation for docking study was initiated by removing water molecules, hetero atoms and co-crystallised ligands from PDB crystal structure of protein 6LU7, polar hydrogen atoms along with Kollman united atom charges were added subsequently to the receptor protein and finally the receptor protein input file was saved as .pdbqt file [49–51]. The three dimensional (3D) structures of ligands (L1-L6) were drawn in Chemsketch (ACD/Structure Elucidator, version 12.01, Advanced Chemistry Development, Inc., Toronto, Canada, 2014, http://www.acdlabs.com.), MM2 program incorporated in Chem Draw Ultra 8.0 were used for geometry optimization of the ligands (L1-L6) and finally, the geometry of ligands (L1-L6) were further optimized with the help of MOPAC 6 package using the semi-empirical AM1 Hamiltonian [52] and structure of each ligand were saved as .pdb file. The input .pdbqt file of the ligands for the docking simulation was generated with the help of Auto Dock Tools (ADT) by assigning required Gasteiger charge and merging non-plolar hydrogen. Molecular structure of ligands L1-L6 is given in Fig. 2.

2.3. Docking study using autodock vina

Auto Dock Vina program 1.1.2 developed by Scripps Research institute were employed for all the molecular docking simulations and BIOVIA Discovery Studio 2020 (DS), version 20.1.0.0 (Dassault Systèmes BIOVIA, Discovery Studio Modeling Environment, Release 2017, San Diego: Dassault Systèmes, 2016) and Edu pymol version 1.7.4.4 were used for the visualization and analysis of docking results and corresponding intermolecular interactions between receptors and the ligand molecules [53–54]. In order to eliminate any biasness arising during the docking study, blind docking of ligand into the protein were carried out by constructing three dimensional (3D) affinity (grid) maps and electrostatic grid boxes of dimension 50 × 50 × 50 Å grid points and grid center (X, Y, Z) of −26.283 12.599 58.966 with a spacing of 1.00 Å with the help of AutoGrid auxiliary program for each of the receptor to cover the entire active site and essential residues within the binding pocket [55]. Lamarckian genetic algorithm was used for all docking simulation and all the torsions were allowed to rotate. The predicted inhibitory constant ($\mathbf{pK_i}$) was estimated using the following standardized equation [56].

$$pK_{i=10^{[\text{Binding Energy Score}/1.336]}}$$

2.4. Synthesis

2.4.1. General procedure for the synthesis of azo imidazole derivatives, L1-L6

Synthesis of azo imidazole derivatives has been achieved by following the literature procedure given elsewhere [38,57–58]. 5 mmol of 1-(2-Aminoethyl)−3-methylimidazolium hexafluorophosphate in absolute ethanol was added to an ethanolic solution of azo-coupled o-vaniline precursors (5 mmol) during a period of 10 min. The reaction mixture was then refluxed in an oil bath for 6 h at 90 °C with constant stirring and the progress of the reaction was monitored by TLC taking 10% ethyl acetate in hexane as eluent. The final solution was kept overnight for cooling and the product obtained was filtered, washed with little ethanol and diethyl ether in a portion (2 ml × 2) respectively. The solid product was recrystallized from hot ethanol solution and dried over silica under vacuum (scheme 1).

The analytical and spectroscopic data for each of the synthesized azo imidazole derivatives are given below:

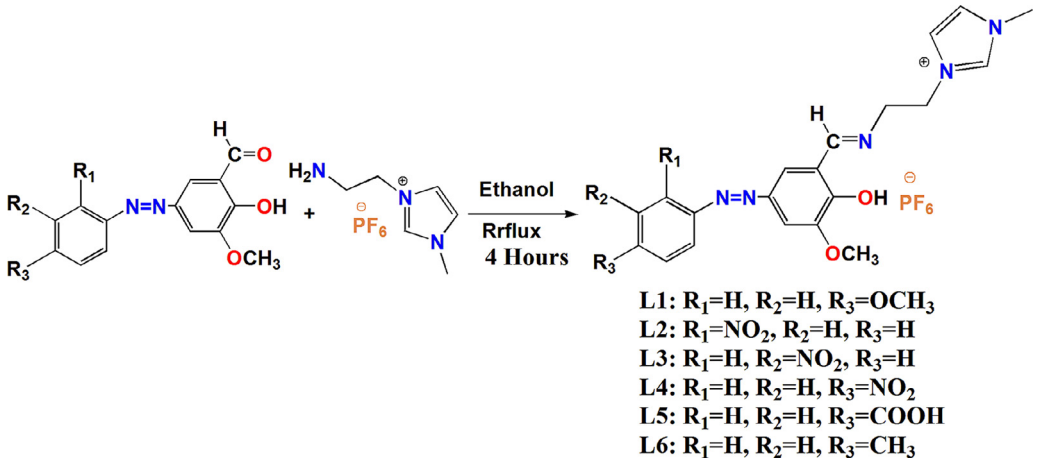

Scheme 1.

2.4.1.1. 1-[2-(2–hydroxy-*3*–methoxy-*5-(4*-methoxyphenylazo) benzaldeneamino)ethyl*]–3-methyl-3H-imidazole-3-ium hexafluorophosphate, (L1).* Red solid. Yield: 68%, (IR, KBr cm^{-1}); 3200–3432(O–H), 1620 (*C = N*), 1602 (*C = C*), 1544, 1502 (*N = N*), 1467, 1253 (C–O), 1148, 975 (*N = N*, bending); 836 (PF_6). ^1H NMR (300 MHz, d_6-DMSO, ppm): δ 4.02 (s, 3H, NCH_3), 3.91 (s, 3H, OCH_3), 3.81 (S, 3H, OCH_3) 3.73 (t, 2H, N–CH_2 J_1=6.00 Hz, J_2=5.30 Hz), 3.81 (t, 2H, N–CH_2, J_1=5.40 Hz, J_2=5.10 Hz), 7.62 (s, 1H, NCH), 7.79 (s, 1H, NCH), 9.15 (s, 1H, N(H) CN), 8.88 (s, 1H, HC=*N*), 12.8 (s, 1H, broad, OH), 7.07–7.87 (m, 6H, Ar-H)) [46–47,59–60]. Anal. calcd. for $C_{21}H_{24}F_6N_5O_3P$: C, 46.76; H, 4.48; F, 21.13; N, 12.98; O, 8.90; P, 5.74. Found: C, 46.52; H, 4.28; F, 21.03; N, 12.78; O, 8.76; P, 5.67%.

2.4.1.2. 1-[2-(2–hydroxy-*3*–methoxy-*5-(2*-nitrophenylazo) benzaldeneamino)ethyl*]–3-methyl-3H-imidazole-3-ium hexafluorophosphate, (L2).* Reddish brown solid. (IR, KBr cm^{-1}); 3167–3433 (O–H), 1638 (*C = N*), 1612 (*C = C*), 1551, 1526 (*N = N*), 1463 (NO_2), 1391, 1351 (NO_2), 1271 (C–O), 1130, 960 (*N = N*, bending); 841 (PF_6). ^1H NMR (300 MHz, d_6-DMSO, ppm): δ 3.33 (s, 3H, NCH_3), 3.95 (s, 3H, OCH_3), 4.11 (t, 2H, N–CH_2 J_1=5.4 Hz, J_2=5.40 Hz), 4.61 (t, 2H, N–CH_2, J_1=6.00 Hz, J_2=5.40 Hz), 7.62 (s, 1H, NCH), 7.78 (s, 1H, NCH), 9.13 (s, 1H, N(H) CN), 8.56 (s, 1H, HC=*N*), 13.3 (s, 1H, broad, OH), 7.26–8.10 (m, 6H, Ar-H)) [46–47,59–60]. Anal. calcd. for $C_{20}H_{21}F_6N_6O_4P$: C, 58.67; H, 5.17; F, 20.56; N, 20.53; O, 15.63; P, 5.59. Found: C, 58.37; H, 5.03; F, 20.51; N, 50.42; O, 15.44; P, 5.53%.

2.4.1.3. 1-[2-(2–hydroxy-*3*–methoxy-*5-(3*-nitrophenylazo) benzaldeneamino)ethyl*]–3-methyl-3H-imidazole-3-ium hexafluorophosphate, (L3).* Reddish brown solid. Yield: 70%, (IR, KBr cm^{-1}); 3436 (O–H), 1635 (*C = N*), 1612 (*C = C*), 1551, 1524 (*N = N*), 1466 (NO_2), 1392, 1351 (NO_2), 1268 (C–O), 1135, 962 (*N = N*, bending); 842 (PF_6). ^1H NMR (300 MHz, d_6-DMSO, ppm): δ 3.37 (s, 3H, NCH_3), 3.98 (s, 3H, OCH_3), 3.86 (t, 2H, N–CH_2 J_1=6.00 Hz, J_2=5.40 Hz), 4.11 (t, 2H, N–CH_2, J_1=6.00 Hz, J_2=5.40 Hz), 7.65 (s, 1H, NCH), 7.88 (s, 1H, NCH), 9.19 (s, 1H, N(H) CN), 8.54 (s, 1H, HC=*N*), 13.8 (s, 1H, broad, OH), 7.35–8.44 (m, 6H, Ar-H) [46–47,59–60]. Anal. calcd. for $C_{20}H_{21}F_6N_6O_4P$: C, 58.67; H, 5.17; F, 20.56; N, 20.53; O, 15.63; P, 5.59. Found: C, 58.47; H, 5.10; F, 20.51; N, 20.43; O, 15.44; P, 5.46%.

2.4.1.4. 1-[2-(2–hydroxy-*3*–methoxy-*5-(4*-nitrophenylazo) benzaldeneamino)ethyl*]–3-methyl-3H-imidazole-3-ium hexafluorophosphate, (L4).* Reddish brown solid. Yield: 70%, (IR, KBr cm^{-1}); 3200–3434 (O–H), 1642 (*C = N*), 1612 (*C = C*), 1551, 1516 (*N = N*), 1458 (NO_2), 1340 (NO_2), 1268 (C–O), 1132, 960 (*N = N*, bending); 847 (PF_6). ^1H NMR (300 MHz, d_6-DMSO, ppm): δ 3.37 (s, 3H, NCH_3), 3.97 (s, 3H, OCH_3), 4.13 (t, 2H, N–CH_2 J_1=6.00 Hz, J_2=4.50 Hz), 4.63 (t, 2H, N–CH_2, J_1=5.70 Hz, J_2=5.40 Hz), 7.65 (s, 1H, NCH), 7.75 (s, 1H, NCH), 9.17 (s, 1H, N(H) CN), 8.60 (s, 1H, HC=*N*), 13.3 (s, 1H, broad, OH), 7.38–8.45 (m, 6H, Ar-H)) [46–47,59–60]. Anal. calcd. for $C_{20}H_{21}F_6N_6O_4P$: C, 43.33; H, 3.82; F, 20.56; N, 15.16; O, 11.54; P, 5.59. Found: C, 43.17; H, 3.77; F, 20.51; N, 15.03; O, 11.44; P, 5.43%.

2.4.1.5. 1-[2-(2–hydroxy-*3*–methoxy-*5-(4*-carboxyphenylazo) benzaldeneamino)ethyl*]–3-methyl-3H-imidazole-3-ium hexafluorophosphate, (L5).* brown solid. Yield: 60%, M.P: (IR, KBr cm^{-1}); 3200–3428 (O–H), 1702 (COOH), 1647 (*C = N*), 1600, (*C = C*), 1459 (*N = N*), 1265 (C–O), 1131, 965 (*N = N*, bending), 838 (PF_6). ^1H NMR (300 MHz, d_6-DMSO, ppm): δ 3.41 (s, 3H, NCH_3), 3.97 (s, 3H, OCH_3), 4.13 (t, 2H, N–CH_2 J_1=5.4 Hz, J_2=5.40 Hz), 4.62 (t, 2H, N–CH_2, J_1=5.7 Hz, J_2=4.8 Hz), 7.66 (s, 1H, NCH), 7.77 (s, 1H, NCH), 9.20 (s, 1H, N(H) CN), 8.62 (s, 1H, HC=*N*), 13.2 (s, 1H, broad, OH), 14.2 (s, 1H, COOH), 7.40–8.14 (m, 6H, Ar-H)) [46–47,59–60]. Anal. calcd. for $C_{21}H_{22}F_6N_5O_4P$: C, 45.58; H, 4.01; F, 20.60; N, 12.66; O, 11.56; P, 5.60. Found: C, 45.44; H, 3.88; F, 20.45; N, 12.53; O, 11.42; P, 5.53%.

2.4.1.6. 1-[2-(2–hydroxy-*3*–methoxy-*5-(4*-methylphenylazo) benzaldeneamino)ethyl*]–3-methyl-3H-imidazole-3-ium hexafluorophosphate, (L6).* Red solid. Yield: 64%, (IR, KBr cm^{-1}); 3200–3428 (O–H), 1645 (*C = N*), 1608 (*C = C*), 1548, 1511 (*N = N*), 1384, 1258 (C–O), 1170, 970 (*N = N*, bending); 840 (PF_6)^1H NMR (300 MHz, d_6-DMSO, ppm): δ 3.70 (s, 3H, NCH_3), 2.35 (s,3H, CH_3), 3.96 (s, 3H, OCH_3), 4.56 (t, 2H, N–CH_2 J_1=5.4 Hz, J_2=5.40 Hz), 4.04 (t, 2H, N–CH_2, J_1=5.7 Hz, J_2=5.10 Hz), 7.66 (s, 1H, NCH), 7.76 (s, 1H, NCH), 9.17 (s, 1H, N(H) CN), 8.61 (s, 1H, HC=*N*), 13.4 (s, 1H, broad, OH), 7.29–7.83 (m, 6H, Ar-H)) [46–47,59–60]. Anal. calcd. for $C_{21}H_{24}F_6N_5O_2P$: C, 48.19; H, 4.62; F, 21.78; N, 13.38; O, 6.11; P, 5.92. Found: C, 48.02; H, 4.55; F, 21.67; N, 13.25; O, 6.03; P, 5.83%.

3. Results and discussion

Condensation of 1-(2-Aminoethyl)–3-methylimidazolium hexafluoro-phosphate, ([2aemim] [PF_6]) with substituted azo-coupled o-vaniline precursors in ethanol resulted in the formation of desired compounds L1-L6. The isolated azo-imidazole compounds (L1-L6) were analyzed using Infrared spectroscopy, NMR spectroscopy and elemental analysis techniques.

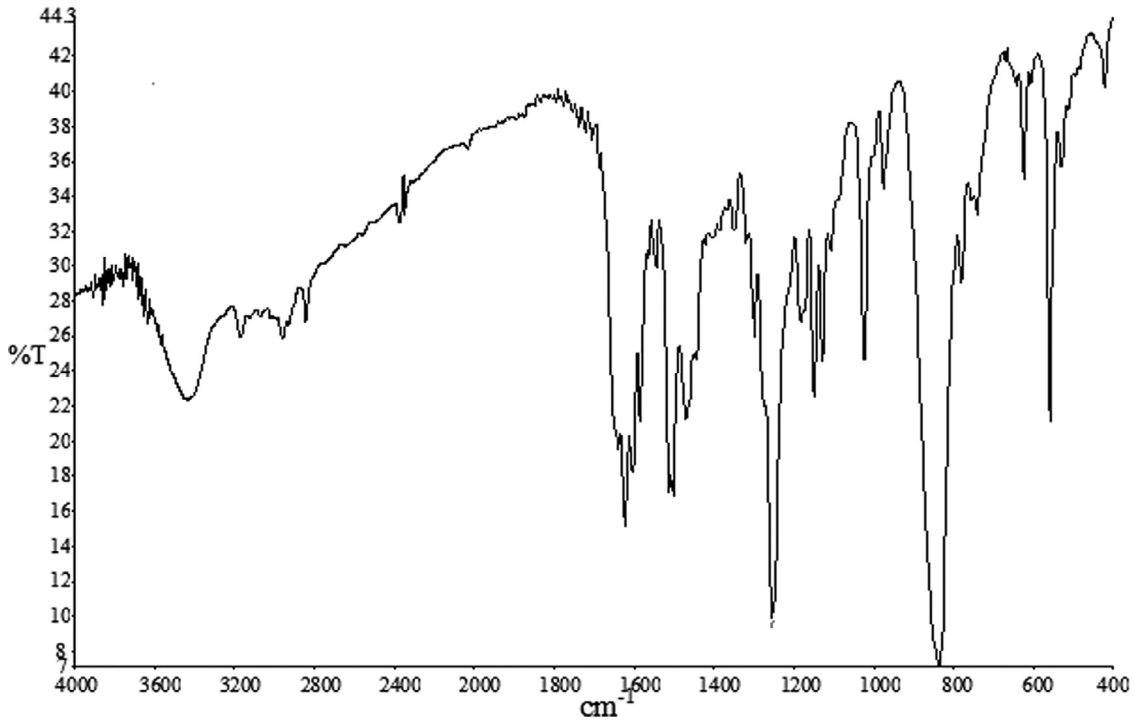

Fig. 3. Infrared Spectra of Compound L1.

3.1. Infrared spectral studies

Infrared spectra measured in the range 400 to 4000 cm^{-1} could provide valuable information regarding the binding mode of the compounds in terms of different specific vibrations. Thus the IR spectra of the synthesized derivatives have been closely analyzed to confirm the formation of the condensation product (L1-L6). In the IR spectrum of the synthesized derivative L1-L6, a band appearing in the range 3428–3436 cm^{-1} can be assigned to the stretching vibration of intra-molecular hydrogen bonded υOH group of compounds (L1-L6) [61]. Also, a stretching frequency in the range 1620–1647 cm^{-1} can be assigned to the stretching vibration of imine linkage $\nu(\text{-}C = N)$ of the synthesized compounds [62–63]. $\nu(C = C)$ stretching frequency of aromatic ring of the compounds (L1-L6) appeared in the range 1602–1612 cm-1 [62]. Two new bands appearing in the region 1544–1551 cm^{-1} and 1459–1526 cm^{-1} can be attributed to υN=*N* stretching frequency and υN=*N* bending vibrations of diazo $(N = N)$ linkage of the compounds (L1-L6) [64]. In the FT-IR spectra of the compound L5, a band at 1702 cm^{-1} can be assigned to the carbonyl stretching frequency of COOH group [65]. A few spectra of the representative compounds (L1 and L5) are depicted in Figs. 3 and 4. A strong band in the range 836–847 cm^{-1} can be attributed for stretching vibration of PF_6 group [59]. Thus the IR spectral data therefore supports the formation of the compounds (L1-L6) and the infrared spectra of other compounds (L2, L3, L4 and L6) are given in supplementary file (Fig S1- Fig S4).

3.2. ^1H nmr spectral studies

The validation of the proposed structure of synthesized product can be achieved by closely analysing FT-NMR spectra of the synthesized azo imidazole derivatives L1-L6. The ^1H NMR of the products L1-L6 were recorded in DMSO–d_6 at ambient temperature and the ^1H NMR spectra associated with the compounds L1-L6 displays a group of signals corresponding to the hydrogen of each molecule. In the ^1H NMR spectrum of L1-L6, a signal of slightly broad singlet peak appearing in the range δ 12.80–13.80 ppm can be assigned to OH proton and a singlet peak at δ14.2 ppm in the ^1H NMR spectra of L5 can be assigned to COOH group [47]. Similarly, the signal appearing in the range δ 8.54–8.88 ppm can be attributed for CH=*N* proton of the compounds L1-L6 [47,57,59,66]. A set of three singlet peaks for imidazole ring NCH proton for all the synthesized derivatives appeared in the range 7.62–7.66 ppm, 7.75–7.79 ppm and 9.13–9.20 ppm respectively. The appearance of the following peaks, triplet in the range δ3.86–4.56 and δ4.04–4.63 can be assigned for aliphatic CH_2–CH_2 protons attached to azometine $(\text{-}C = N)$ linkage [58]. Two singlet peaks appearing in the range 3.33–4.01 ppm and 3.91–3.98 ppm can be assigned for the CH_3 proton attached to imidazole ring and OCH_3 proton in the compounds L1-L6 respectively. The NMR spectra of the representative compounds L1 and L5 are shown in Figs. 5 and 6 respectively. The signal for CH_3 proton of L6 appeared at δ 2.35 ppm. Appearance of multiplate signals in the range δ 7.07–8.45 ppm can be assigned for aromatic protons belonging to synthesized compounds (L1-L6). The NMR spectra of other compounds (L2 and L4) are listed in supplementary file (Fig S5 – Fig S6).

3.3. In silico pharmacokinetics analysis of L1-L6

Prior to clinical and animal studies, any substance or compound to be categorized as drug candidate, the pharmacokinetic properties like absorption, distribution, metabolism, excretion and toxicity (ADMET) of the candidate compound are fundamental parameters as it determines the drug likeness as well as activity inside the body of the studied compound [67]. Also, the Pharmacokinetics parameters provide valuable information about concentrations of drug in the different parts of the body with respect to time [68]. The pharmacokinetic properties such as gastrointestinal absorption (GI), water soluble capability (Log S), lipophilicity (LogPo/W), CYP1A2 inhibitor and Blood - Brain Barrier (BBB) are very important for any compound to be considered as a drug candidate [69]. Therefore, the pharmacokinetic properties of the studied ligands

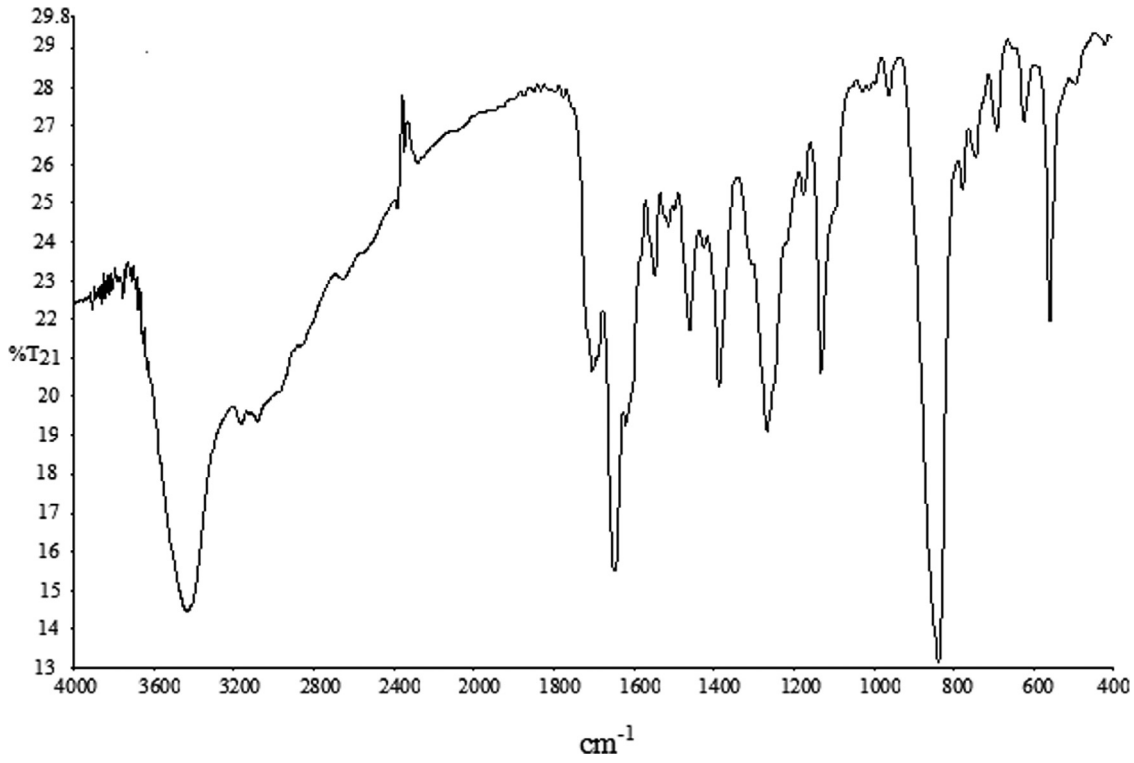

Fig. 4. Infrared Spectra of Compound L5.

Table 1
Lipinski's properties and pharmacokinetic properties (ADME) of the ligands L1-L6.

Properties	L1	L2	L3	L4	L5	L6
Molecular weight (gm/mole)	394.45	410.43	410.43	410.43	408.43	378.45
Rotatable bonds	8	8	8	8	8	7
H-bond donor (5)	1	2	2	2	2	1
H-bond acceptor	6	7	7	7	7	5
Violations	0	0	0	0	0	0
Log Po/W	2.36	1.75	1.75	1.75	2.03	2.69
Log S	−3.90 (MS)	−3.61 (MS)	−3.61 (MS)	−3.61 (MS)	−3.69 (MS)	−4.13 (MS)
GI	High	Low	Low	Low	High	High
BBB	No	No	No	No	No	No
CYP1A2	No	No	No	No	No	No
Bioavailability Score	0.55	0.55	0.55	0.55	0.56	0.55
Topological Surface Area (Å^2)	85.63	126.06	126.06	126.06	113.70	76.40

*MS: Moderately Soluble, BBB: Blood-Brain Barrier, CYP: Cytochrome P450, GI: Gastrointestinal tract.

(L1-L6) have been determined with the help of computer aided online SwissADME database (http://www.sib.swiss) and the result of pharmacokinetic properties as well as Lipinski's property are depicted in Table 1.

Analysis of Table 1 have revealed that all the studied compounds (L1-L6) with bioavailability in the range 55–56% have consensus lipophilicity (LogPo/W) value in the range 1.75–2.69 and all the compounds showed good gastrointestinal absorption (GI) except ligand L4, no CYP1A2 and blood brain barrier (BBB) penetration properties. Thus the high and positive lipophilicity values (LogPo/W) for all the studied ligands indicates that they are more lipophilic and all the compounds could easily pass through the lipid bilayer of most cellular membrane [69]. However, the solubility parameter (LogS) of the compounds (L1-L6) fall in the range −3.62 to −4.13 and it suggest that the studied compounds are moderately soluble in water. Hence, the pharmacokinetic parameters suggest that the studied ligands (L1-L6) could serve as a potential drug candidate with no Lipinski's rule violation and the ligands (L1-L6) qualifies the drug likeness criteria.

3.4. Molecular docking study

Computer aided drug designing especially molecular docking and molecular dynamic method have proven to be an efficient technique to screen the potential drug candidate against specific disease [70]. Molecular docking study provides an insight into the effectiveness of binding of ligands against the studied receptor protein. Again, recent studies have shown that the main protease (M^{pro}) of SARS-CoV-2 have been found to consist of three domain viz., domain I (residues 8–101), domain II (residues 102–184) and domain III (residues 201–303) and as similar to other coronaviruses, SARS-CoV-2 Mpro also consist a Cys145-His41 catalytic dyad located in a cleft between domain I and domain II (Fig. 7) [71–75].

The Cys-His-catalytic dyad of M^{pro} have been found to show protease activity [76–77]. Thus, inhibition of catalytic dyad in M^{pro} could an effective and attractive target for designing and screening of anti-Cov drug [78]. Till date no therapeutic agents or vaccine is available to treat the infection caused by SARS-CoV-2 and only

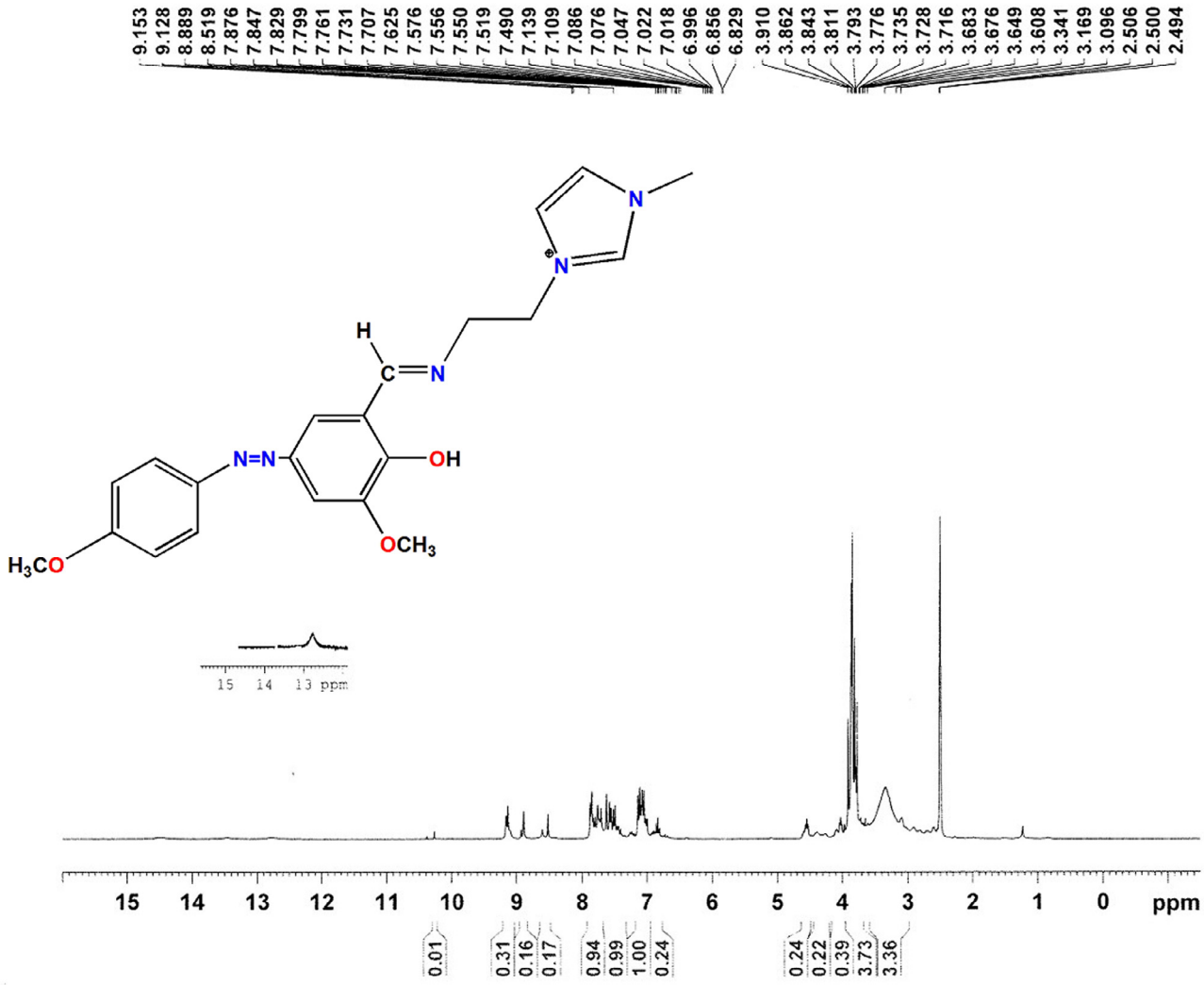

Fig. 5. ^{1}H NMR spectra of compound L1.

several FDA approved and clinically trial antiviral, anti HIV and anti Malarial drugs are available as supportive measures to treat SARS-CoV-2 infection [79–81]. Molecular docking and molecular dynamic simulation methods provides an alternative way to screen the potential drug candidates for the specific disease at relatively less time [82]. Therefore, in this research work, we are utilizing the molecular docking method to study the efficiency of novel azo imidazole derivatives (L1-L6) as inhibitors against M^{pro} of SARS-CoV-2. The results obtained from the docking studies have shown that the ligands (L1-L6) interacts with main protease, M^{pro} of SARS-CoV-2 near the cleft between domain I and domain II except for L2 (cleft between domain II and domain III). A summary of the results obtained from docking of studied ligands (L1-L6) with main protease (M^{pro}, 6LU7) are summarized in Table 2.

3.5. Visualization of docking results

Recent studies on SARS-CoV and SARS-CoV-2 have shown that the amino acid residues His41, Cyd145 and Glu166 are important residues in substrate binding site and the residues Cys145-His41 forms the catalytic dyad. More interestingly, these residues in catalytic dyad could be the most prominent and potential target for the inhibitory effect of main protease (M^{pro}) [83]. After successful docking of all the ligands (L1-L6) with M^{pro} of SARS-CoV-2, the docking results showed various modes of significant protein ligand interactions with particular binding energies. The ligands are shown as blue green stick model and the protein is shown as surface to understand the fitting of ligands in the binding pocket. The hydrogen bonding interactions are represented by green dash line and pi-sulfer interaction is represented by yellow dash line. The amino acids involved in the protein-ligand interactions are shown as stick with different color. From, the molecular docking study, the binding energies (ΔG) and predicted inhibitory constant (pK_i) of the ligands (L1-L6) are found to be −7.7 Kcal/mole (L1), −7.4 Kcal/mole (L2), −6.7 kcal/mole (L3), −7.9 Kcal/mole (L4), −8.1 Kcal/mole (L5) and −7.9 Kcal/mole (L6) respectively and 1.72 μM, 2.89 μM, 9.66 μM, 1.22 μM, 0.86 μM and 1.22 μM respectively.

The interaction of L1 with the Protease (6LU7) showed high affinity interaction as the ligand L1 fits inside the core pocket region of the protease at the interface between domain I and domain II (Fig. 8). A closed analysis of the binding of L1 with the protein 6LU7 revealed that the L1 binds to the protein with binding energy (ΔG) −7.7 Kcal/mole and the predicted inhibitory constant found to be 1.72 μM. The major interaction between L1 and the protein 6LU7 are characterized by three hydrogen bonding between NH (Imidazole ring) group of residue His41 and N atom of azo linkage ($N = N$) at a distance 2.74 Å, NH_2 group of residue Gly143 and O atom of OH group of L1 at a distance 2.52 Å and $C = O$ group of residue Ser144 with proton (H) of

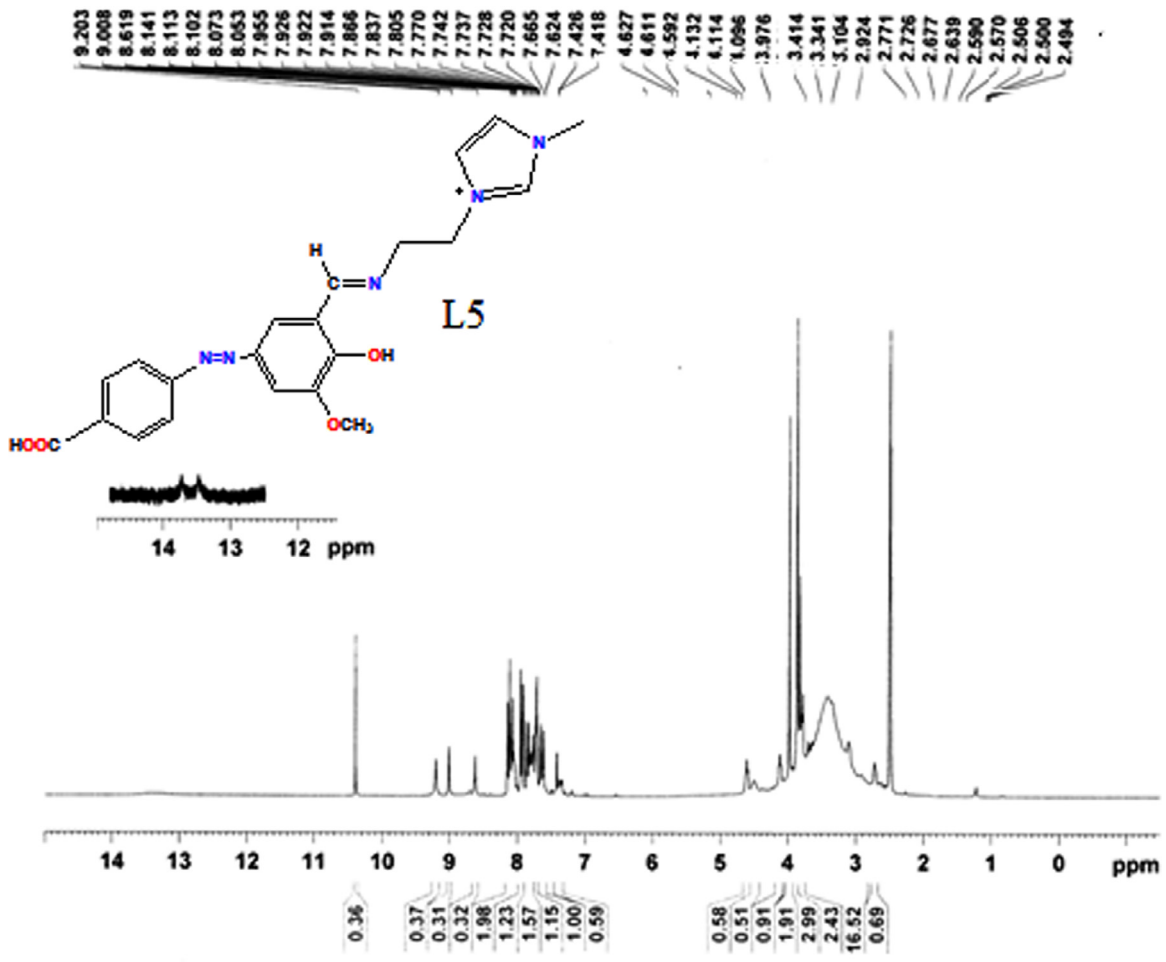

Fig. 6. ^{1}H NMR spectra of compound L5.

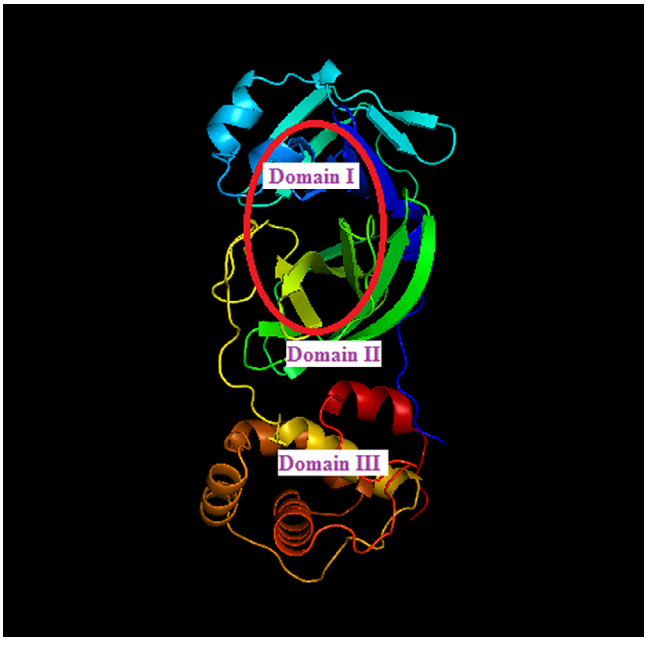

Fig. 7. Structure (Chain A) of M^{pro} of SARS-Cov-2 with domain I, II and III (Red circle represents the catalytically active site of M^{pro}).

OH group at a distance 2.98 Å respectively (Fig. 8). The amino acid residue His163, Met165 and His 172 interacts with the ligand L1 through π-alkyl (π electron of amino acid residues and OCH_3 group of L1) interactions. Apart from these interactions, π-donor hydrogen bonds are formed by the residues Thr24, Thr26, Phe140 and Cys145. Some van der walls interactions between the residues Thr25, Leu27, Thr45, Met49, Asn142, Glu160, Gln189 and Thr190 and L1 has been observed. Also an unfavorable acceptor interaction has been observed between the ligand and the residue Leu141.

Analysis of docking result of ligand L2 with protein 6LU7 revealed that the ligand binds with the protein at the interface between domain II and domain III with binding energy −7.4 Kcal/mole and predicted inhibitory constant 2.89 μM. A close inspection of the docking result showed that the ligand L2 binds with the protein with three favorable hydrogen bonding interactions. The hydrogen bonds are formed between, NH_2 group of amino acid residue Gln110 and N atom of azomethine group ($C = N$) of L2 at a distance 2.50 Å, NH_2 group of amino acid residue Asn151 and NO_2 group of L2 at a distance 1.95 Å and OH group of residue Ser158 and NO_2 group of L2 at a distance 3.08 Å respectively (Fig. S7). Amino acid residue Phe294 found to interact through π-π stacking interactions between the π-electron of Phe294 and π-electron of L2 at a distance 4.26 Å. The other types of interactions such as π-σ (Ile106 and NO_2 group of L2) interaction, π-alkyl (Phe8, Val104 and OCH_3 group of L2) interaction and

Table 2
Summary of docking of ligand (L1-L6) against COVID-19 Main Protease (M^{pro}, 6LU7) with their binding energy (ΔG), predicted inhibitory constant ($\mathbf{pK_i}$), interacting amino acid residues and types of interactions.

Ligands	Binding Energy (Kcal/mole)	Predicted inhibitory constant ($\mathbf{pK_i}$) μM	Amino Acid residues	Types of interactions
L1	−7.7	1.72	His41, Gly143 and Ser144	H-bonding
			His163, Met165 and His172	π-alkyl
			Thr24, Thr26, Phe140 and Cys145	π-donor H bond
			Thr25, Leu27, Thr45, Met49, Asn142, Glu160, Gln189 and Thr190	Van der walls
			Leu141	Unfavorable Acceptor- acceptor
L2	−7.4	2.89	Gln110, Asn151 and Ser158	H-bond
			Phe294	π-π stacked
			Ile106	π-sigma (σ)
			Phe8 and Val104	π-alkyl
			Gln107, Thr111, Asp153, Cys160, Val202, His246, Ile249, Thr292 and Pro293	Van der walls
L3	−6.7	9.66	Ser144, His163, Glu166, Thr190 and Gln192	H-bond
			Met165	π-sulpher
			Cys145	π-alkyl
			Phe140, leu141, Asn142, Gly143, His172, Arg188, Gln189 and Ala191	Van der walls
L4	−7.9	1.22	His41, leu141 and cys145	H-bond
			His163 and His172	π-alkyl
			Thr24, Thr26 and Phe140	π-donor H bond
			Thr25, Leu27, Thr45, Met49, Phe140, Asn142, Gly143, Ser144, Met165, Glu166, Pro168 and Thr190	Van der walls
L5	−8.1	0.86	His41, Leu141, Cys145 and Glu166	H-bond
			Met165	π-sulpher
			His163 and His172	π-alkyl
			Thr24, Thr25, Thr26 and Phe140	π-donor H bond
			Leu27, Thr45, Met49, Asn142, Gly143, Ser144, Pro168, Gln189, Thr190 and Ala191	Van der walls
L6	−7.9	1.22	Leu141, Gly143, Ser144 and Cys145	H-bonding
			Met165	π-sulpher
			His163 and His172	π-alkyl
			Thr24, Thr26 and Phe140	π-donor H bond
			Thr25, Leu27, His41, Met49, Asn142, Glu166, Gln189 and Thr190	Van der walls

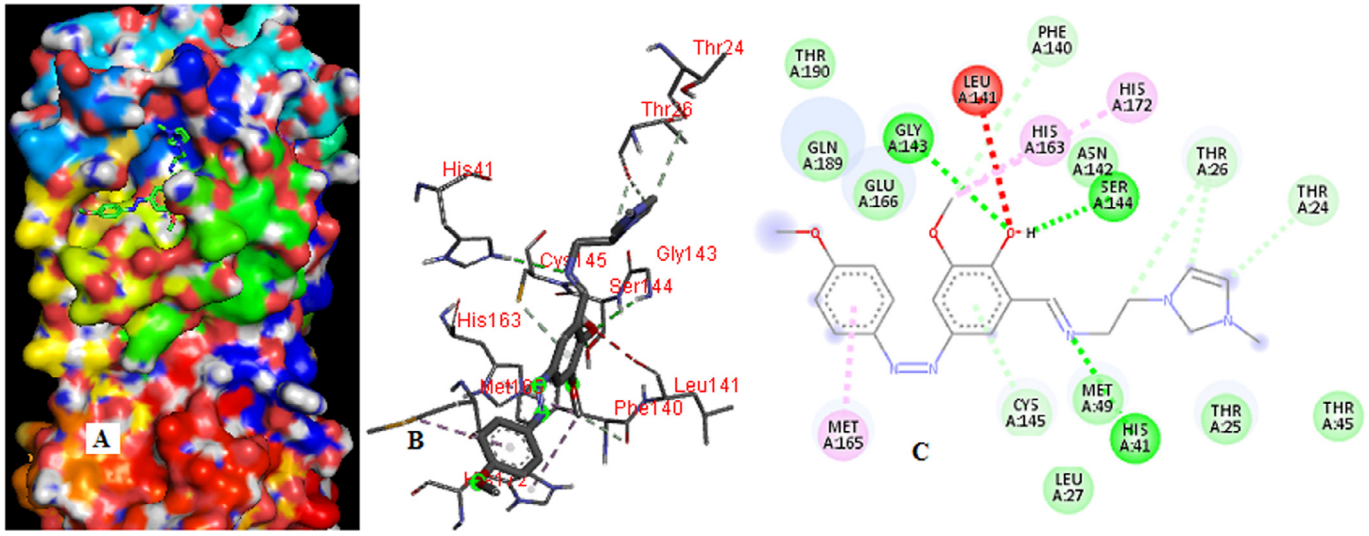

Fig. 8. Visualization of docking of Ligand L1 docked in M^{pro} (6LU7): (A) Best binding mode of protein (Ligand L1 as green and blue stick), (B) Amino acid residues involved in hydrogen bonding interaction (green dash line represents H-bonding, people and green color represents donor and acceptor) and (C) Binding interaction (2D) of ligand L1 with amino acid residues of protein 6LU7 (green dash line represents H-bonding and red dash line represents unfavorable acceptor-aceptor interaction).

Van der walls (residues Gln107, Thr111, Asp153, Cys160, Val202, His246, Ile249, Thr292 and Pro293) interactions are found to exist between ligand L2 and protein 6LU7.

Result obtained by docking of L3 with protein 6LU7 revealed that the ligand L3 fits inside the core pocket region (at interface between domain I and domain II) of protein with binding energy −6.7 Kcal/mole and predicted inhibitory constant 9.66 μM. The ligand L3 interacts with the protein 6LU7 through five hydrogen bonding interactions. These hydrogen bonds are formed between (i) OH group of residue Ser144 and NO_2 group of L3 at a distance 2.85 Å, (ii) NH (imidazole ring) group of residue His163 and NO_2 group of L3 at a distance 1.96 Å, (iii)NH(amide) group of residue Glu166 and azo ($N = N$) linkage of L3 at a distance 2.49 Å, (iv) $C = O$ group of residue Thr190 and proton (H) of OH group of L3 at a distance 2.15 Å and (v) NH_2 group of residue Gln192 and O atom of OCH_3 group of L3 at a distance 2.78 Å respectively. The S atom of amino acid residue Met165 forms π-sulpher interaction with π electron of L3 at a distance 5.07 Å (Fig.S8). The amino acid residue

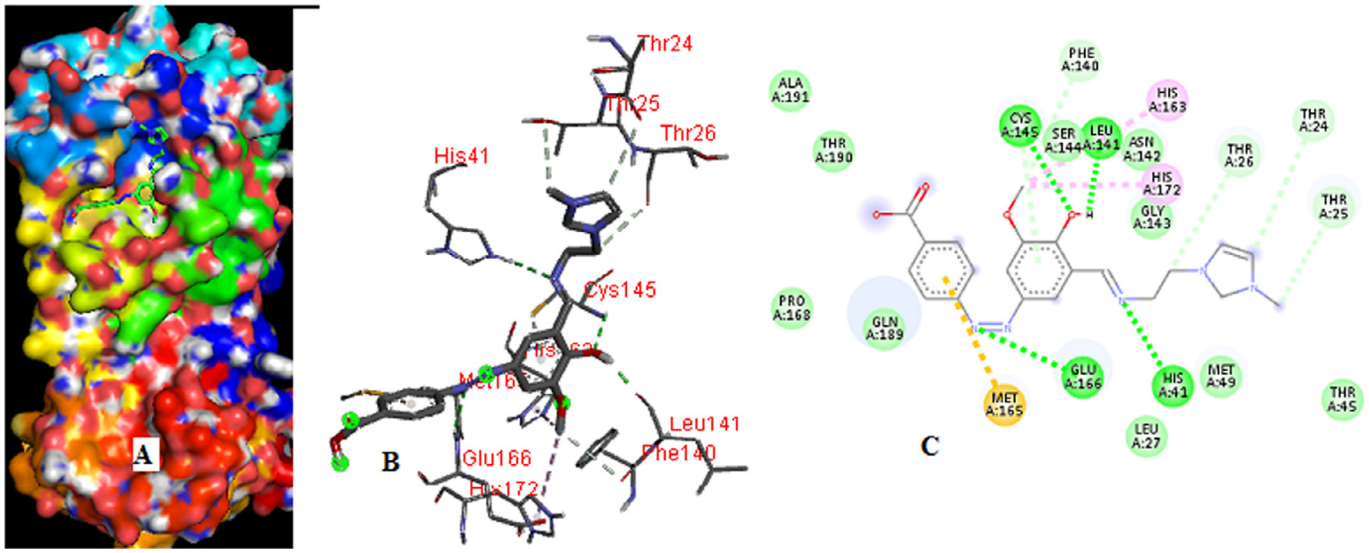

Fig. 9. visualization of docking of ligand L5 docked in M^{pro} (6LU7) (A) Best binding mode of protein (Ligand L5 as green and blue stick), (B) interacting amino acid residues involved in hydrogen bonding (green dash line represents H-bonding) and (C) two dimensional (2D) view of binding interaction of ligand L5 with amino acid residues of protein 6LU7 (green dash line represents H-bonding and yellow dash line represents π- sulpher interaction).

forms Pi-alkyl interaction with OCH_3 group of L3. The amino acid residues Phe140, Leu141, Asn142, Gly143, His172, Arg188, Gln189 and Ala191 are found to interact with the ligand L3 through Van der walls interactions.

The docking of ligand L4 with COVID-19 main protease (6LU7) revealed that the L4 interacts with the protein through three favorable hydrogen bonding with binding energy (ΔG) −7.9 Kcal/mole and predicted inhibitory constant 1.22 μM. The ligand L4 found to interact with the protein through two hydrogen bonds at the catalytic dyad (Cys145-His41) in the interface between domain I and domain II. The NH (imidazole ring) group of residue His41 form hydrogen bond with N atom of azomethine ($C = N$) group of L4 at a distance 2.80 Å and similarly, NH_2 group of residue Cys145 form hydrogen bond with O atom of OH group of L4 at a distance 2.63 Å. The other hydrogen bond exist between the $C = O$ group of residue Leu141 and proton (H) of OH group of L4 at a distance 1.83 Å (Fig. S9). Also, the π electron of residues His163 and His172 forms π-alkyl interaction with OCH_3 group of L4. Apart from these interactions, other interactions such as π-donor H bond between the residues Thr24 and Thr26 and ligand L4 and Van der walls interactions between the ligand L4 and residues Thr25, Leu27, Thr45, Met49, Phe140, Asn142, Gly143, Ser144, Met165, Glu166, Pro168 and Thr190 also exist.

Docking of ligand L5 docked in COVID-19 protease (6LU7) revealed that the ligand L5 has the highest binding affinity among all the studied ligands (L1-L6) with binding energy (ΔG) −8.1 Kcal/mole and predicted inhibitory constant 0.86 μM. The ligand L5 shows significant interactions in the region of interface between Domain I and Domain II. The ligand L5 forms strong hydrogen bond network with the protein 6LU7. Close analysis of docking result showed that the ligand forms four hydrogen bonds with the protein residues. The two hydrogen bonds have been found to exist at the catalytic (Cys145-His41) dyad at the interface between Domain I and Domain II of the protein. The NH(imidazole ring) group of residue His41 form hydrogen bond with N atom of azomethine ($C = N$) group of L5 at a distance 2.95 Å and similarly, NH_2 group of residue Cys145 form hydrogen bond with OH group of L5 at a distance2.65 Å. The other two hydrogen bond exist between, $C = O$ group of residue Leu141 and proton (H) of OH group of L at a distance 1,86 Å and NH (amide) group of residue Glu166 and azo ($N = N$) linkage of L5 at a distance 2.81 Å (Fig. 9). Apart from hydrogen bonding, S atom of residue Met165 form π-sulpher interactions with π electron of ligand L5 at a distance 5.32 Å. The other types of interaction such as π- alkyl between π-electron of residue His163 and His172 and OCH3 group of L5, π-donor hydrogen bonding between the residues Thr24, Thr25, Thr26 and Phe140 and L9 and some van der walls interactions between the residue Leu27, Thr45, Met49, Asn142, Gly143, Ser144, Pro168, Gln189, Thr190 and Ala191 and ligand L5 have also been observed.

With four major hydrogen bonds, ligand L6 binds in the region between Domain I and Domain II and showed significant activity with main protease (6LU7) of SARS-CoV-2. The docking result revealed that L6 binds with the protein with binding energy (ΔG) −7.9 Kcal/mole and predicted inhibitory constant 1.22 μM. The four major hydrogen bonds are formed between, (i) $C = O$ group of residue Leu141 and proton (H) of OH group of L6 at a distance 2.74 Å, (ii) NH_2 group of residue Gly143 and O atom of OH group of L6 at a distance 2.56 Å, (iii) OH group of residue Ser144 and proton (H) of OH group of L6 at a distance 2.38 Å and (iv) NH_2 group of residue Cys145 and O atom of OH group of ligand L6 at a distance 2.65 Å respectively (Fig. S10). S atom of amino acid residue Met165 form π-sulpher interactions with π electron of ligand L6 at a distance 5.60 Å. Apart from these interactions, other interactions such as π- alkyl (between π electron of residue His163 and His172 and OCH_3 group of L6), π-donor hydrogen bond (between residues Thr24, Thr26 and Phe140 and L6) and Van der walls interactions (between the residues Thr25, leu27. His41, Met49, Asn142, Glu160, Gln189 and Thr190 and ligand L6) have also been observed.

4. Conclusion

Six novel azo imidazole derivatives were synthesized in good yields and the products have been characterized by different analytical and spectroscopic tools. Molecular docking study of all the synthesized derivatives have been studied against the main protease (6LU7) of SARS-CoV-2. The docking results attributed various types of protein- ligand interactions and it is also seen that the ligands shows significant interactions at the interface between domain I and domain II except for ligand L2. Furthermore, most of the ligands showed interaction at the Cys145-His41 catalytic dyad. The pharmacokinetic study (ADMET) has revealed that the ligands

(L1-L6) could act as a potential drug candidate. Therefore, we may conclude that the ligands (L1-L6) could act as potential inhibitor against the main protease (6LU7) of SARS-CoV-2 and the affinity of ligands (L1-L6) towards the main protease of SARS-CoV-2 follows the order L5> L4≈L6>L1>L2>L3.

Declaration of Competing Interest

The authors do not declare any conflict of interest. The authors declare no conflict of interest associated with this article and also no significant financial support has been received by us for preparing this manuscript.

CRediT authorship contribution statement

Abhijit Chhetri: Conceptualization, Formal analysis, Funding acquisition, Software, Validation, Writing - original draft, Writing - review & editing. **Sailesh Chettri:** Data curation, Formal analysis, Funding acquisition, Investigation, Methodology, Writing - original draft. **Pranesh Rai:** Methodology, Project administration, Validation. **Dipu Kumar Mishra:** Data curation, Investigation, Validation, Writing - review & editing. **Biswajit Sinha:** Conceptualization, Methodology, Project administration, Supervision, Visualization, Writing - review & editing. **Dhiraj Brahman:** Conceptualization, Data curation, Formal analysis, Funding acquisition, Investigation, Methodology, Project administration, Software, Supervision, Validation, Visualization, Writing - original draft, Writing - review & editing.

Acknowledgements

The authors are grateful to the research facilities available at the St. Joseph's College, Darjeeling and University of North Bengal, Darjeeling. All the authors sincerely acknowledge SAIF, NEHU, Shilong, India for NMR and elemental analysis.

Supplementary materials

Supplementary material associated with this article can be found, in the online version, at doi:10.1016/j.molstruc.2020.129230.

References

[1] N. Zhu, D. Zhang, W. Wang, X. Li, B. Yang, J. Song, X. Zhao, B. Huang, W. Shi, R. Lu, P. Niu, F. Zhan, X. Ma, D. Wang, W. Xu, G. Wu, G.F. Gao, W. Tan, A novel coronavirus from patients with pneumonia in China, 2019, New Eng. J. Med. 382 (2020) 727–733, doi:10.1056/NEJMoa2001017.

[2] C. Huang, Y. Wang, X. Li, L. Ren, J. Zhao, Y. Hu, L. Zhang, G. Fan, J. Xu, X. Gu, Z.C. Cheng, T. Yu, J. Xia, Y. Wei, W. Wu, X. Xie, W. Yin, H. Li, M. Liu, Y. Xiao, H. Gao, L. Guo, J. Xie, G. Wang, R. Jiang, Z. Gao, Q. Jin, J. Wang, B. Cao, Clinical features of patients infected with 2019 novel coronavirus in Wuhan, China, Lancet 395 (2020) 497–506, doi:10.1016/S0140-6736(20)30183-5.

[3] S. Su, G. Wong, W. Shi, J. Liu, A.C.K. Lai, J. Zhou, W. Liu, Y. Bi, G.F Gao, Epidemiology, genetic recombination, and pathogenesis of coronaviruses, Trends in Microbiol. 24 (6) (2016) 490–502, doi:10.1016/j.tim.2016.03.003.

[4] C.R. MacIntyre, Global spread of COVID-19 and pandemic potential, Global Biosecurity 1 (3) (2020), doi:10.31646/gbio.55.

[5] A. Wu, Y. Pen, B. Huang, X. Ding, X. Wang, P.N. Jing, Z.Z. Zhu, J. Wang, J. Sheng, L. Quan, X. Xia, W. Tan, G. Cheng, T. Jiang, Genome Composition and Divergence of the Novel Coronavirus (2019-nCoV) Originating in China, Cell Host Microbe 27 (2020) 325–328, doi:10.1016/j.chom.2020.02.001.

[6] X. Liu, S. Zhang, COVID-19: face masks and human-to-human transmission, in: Influenza Other Respiratory Viruses, 14, Wiley, 2020, pp. 472–473, doi:10.1111/irv.12740.

[7] Y.-.R. Guo, Cao Q-D, Z.-.S. Hong, Y.-.Y. Tan, S.-.D. Chen, H.-J. Jin, K.-.S. Tan, Dd-Y. Wang, Y. Yan, The origin, transmission and clinical therapies on coronavirus disease 2019 (COVID-19) outbreak – an update on the status, Military Med. Res. 7 (11) (2020) 1–10, doi:10.1186/s40779-020-00240-0.

[8] W.H. Li, M.J. Moore, N. Vasilieva, J.H. Sui, S.K. Wong, M.A. Berne, M. Somasundaran, J.L. Sullivan, K. Luzuriaga, T.C. Greenough, H. Choe, M. Farzan, Angiotensin-converting enzyme 2 is a functional receptor for the SARS coronavirus, Nature 426 (2003) 450–454, doi:10.1038/nature02145.

[9] M.L. Sun, J.M. Yang, Y.P. Sun, G.H. Su, Inhibitors of RAS Might Be a Good Choice for the Therapy of COVID-19 Pneumonia, Chin. J. Tuberculo. & Respire. Dis. 43 (3) (2020) 219-222, doi:10.3760/cma.j.issn.1001-0939.2020.03.016.

[10] V.K. Maurya, S. Kumar, M. Bhatt, S.K. Saxena, Therapeutic Development and Drugs for the Treatment of COVID-19, in: Coronavirus Disease 2019 (COVID-19): Epidemiology, Pathogenesis, Diagnosis, and Therapeutics, 2020, pp. 109–126, doi:10.1007/978-981-15-4814-7-10.

[11] P.I. Andersena, A. Ianevskia, H. Lysvanda, A. Vitkauskieneb, V. Oksenycha, M. Bjøråsa, K. Tellingc, I. Lutsard, U. Dumpise, Y. Iriec, T. Tensonc, T. Kantelef, D.E. Kainov, Discovery and development of safe-in-man broad-spectrum antiviral agents, Int. J. Infect. Dis 93 (2020) 268–276, doi:10.1016/j.ijid.2020.02.018.

[12] R. Wu, L. Wang, H-C.D. Kuo, A. Shannar, R. Peter, P.J. Chou, S. Li, R. Hudlikar, X. Liu, G.J. Poiani, L. Amorosa, L. Brunetti, A.-.N. Kong, an Update on Current Therapeutic Drugs Treating COVID-19, Curr. Pharmacol. Rep. 6 (2020) 56–70, doi:10.1007/s40495-020-00216-7.

[13] Z. Lv, Y. Chu, Y. Wang, HIV protease inhibitors: a review of molecular selectivity and toxicity, HIV/AIDS (Auckland, New Zealand) 7 (2015) 95–104, doi:10.2147/HIV.S79956.

[14] P. de Leuw, C. Stephan, Protease inhibitors for the treatment of hepatitis C virus infection, GMS Infect. Dis. 5 (2017) 1–14 Doc08, doi:10.3205/id000034.

[15] H. Nishimura, M Yamaya, A Synthetic Serine Protease Inhibitor, Nafamostat Mesilate, Is a Drug Potentially Applicable to the Treatment of Ebola Virus Disease, The Tohoku J. Exp. Med. 237 (1) (2015) 45–50, doi:10.1620/tjem.237.45.

[16] A. Zumla, J.F. Chan, E.I. Azhar, D.S. Hui, K.Y Yuen, Coronaviruses - drug discovery and therapeutic options, Nat. Rev. Drug. Discov. 15 (5) (2016) 327–347, doi:10.1038/nrd.2015.37.

[17] K. Shirato, M. Kawase, S. Matsuyama, Middle East respiratory syndrome coronavirus infection mediated by the transmembrane serine protease tmprss2, J. Virol. 87 (23) (2013) 12552–12561, doi:10.1128/JVI.01890-13.

[18] R. Hatada, K. Okuwaki, Y. Mochizuki, Y. Handa, K. Fukuzawa, Y. Komeiji, Y. Okiyama, S. Tanaka, Fragment molecular orbital based interaction analyses on COVID-19 main protease- inhibitor N3 complex (PDB ID: 6LU7), J. Chem. Inf. Model. 60 (7) (2020) 3593–3602, doi:10.1021/acs.jcim.0c00283.

[19] M.T. ul Qamar, A. Maryam, I. Muneer, F. Xing, U.A. Ashfaq, F.A. Khan, F. Anwar, M.H. Geesi, R.R. Khalid, S.A. Rauf, A.R. Siddique, Computational screening of medicinal plant phytochemicals to discover potent pan-serotype inhibitors against dengue virus, Sci. Rep. 9 (1) (2019) 1–16, doi:10.1038/s41598-018-38450-1.

[20] M.T. ul Qamar, S. Saleem, U.A. Ashfaq, A. Bari, F Anwar, S Alqahtani, Epitope-based peptide vaccine design and target site depiction against Middle East Respiratory Syndrome Coronavirus: an immune-informatics study, J. Transl. Med. 17 (362) (2019) 1–14, doi:10.1186/s12967-019-2116-8.

[21] M. Gaba, C. Mohan, Development of drugs based on imidazole and benzimidazole bioactive heterocycles: recent advances and future directions, Med. Chem. Res. 25 (2016) 173–210, doi:10.1007/s00044-015-1495-5.

[22] M. Saudi, J. Zmurko, S. Kaptein, J. Rozenski, J. Neyts, A.V. Aerschot, Synthesis and evaluation of imidazole-4,5- and pyrazine-2,3- dicarboxamides targeting dengue and yellow fever virus, Eur. J. Med. Chem. 87 (2014) 529–539, doi:10.1016/j.ejmech.2014.09.062.

[23] E.V. Aleksandrova, A.N. Kravchenko, P.M. Kochergin, Properties of haloimidazoles, Chem. Heterocycl. Compd. 47 (2011) 261–289, doi:10.1007/s10593-011-0754-8.

[24] L. Zhang, X.-.M. Peng, G.L.V. Damu, R.-.X. Geng, C.-.H. Zhou, Comprehensive Review in Current Developments of Imidazole-Based Medicinal Chemistry, Med. Res. Rev. 34 (2) (2013) 340–437, doi:10.1002/med.

[25] M. Fujiu, S. Sawairi, H. Shimada, H. Takaya, Y. Aoki, T. Okuda, K. Yokose, Azoxybacilin, a novel antifungal agent produced by Bacillus cereus NR2991. Production, isolation and structure elucidation, J. Antibiot. (Tokyo) 47 (7) (1994) 833–835, doi:10.7164/antibiotics.47.833.

[26] T. Iwamoto, E. Tsujii, M. Ezaki, A. Fujie, S. Hashimoto, M. Okuhara, M. Kohsaka, H. Imanaka, K. Kawabata, Y. Inamoto, FR109615, a new antifungal antibiotic from Streptomyces setonii. Taxonomy, fermentation, isolation, physicochemical properties and biological activity, J. Antibiot. (Tokyo) 43 (1) (1990) 1–7, doi:10.7164/antibiotics.43.1.

[27] S. Omura, K. Otoguro, N. Imamura, H. Kuga, Y. Takahasi, R. Masuma, Y. Tanaka, H. Tanaka, S. Xue-Hui, Y En-Tai, Jietacins, A and B, new nematocidal antibiotics from a streptomyces sp, J. Antibiot. (Tokyo) 40 (5) (1987) 623–629, doi:10.7164/antibiotics.40.623.

[28] M. Umezawa, T. Takeuchi, H. iinuma, M. Ito, M. Ishizuka, Y. Kurakata, Y. Umeda, Y. Nakanishi, T. Nakamura, A. Obayashi, O Tanabe, A New Antibiotic, Calvatic Acid, J. Antibiot. (Tokyo) 28 (1) (1975) 87–90, doi:10.7164/antibiotics.28.87.

[29] N. Hahon, Inhibition of viral interferon induction in mammalian cell cultures by azo dyes and derivatives activated with rat liver S9 fraction, Environ. Res. 37 (1) (1985) 228–238, doi:10.1016/0013-9351(85)90060-x.

[30] A. Martıńez, A.I. Esteban, A. Herrero, C. Ochoa, G. Andrei, R. Snoeck, J. Balzarini, E.D. Clercq, Imidazothiadiazine dioxides: synthesis and antiviral activity, Bioorgan. Med. Chem. 7 (8) (1999) 1617–1623, doi:10.1016/S0968-0896(99)00114-5.

[31] A.H. Shridhar, J. Keshavayya, S.K. Peethambar, H. Joy Hoskeri, Synthesis and biological activities of Bis alkyl 1, 3, 4-oxadiazole incorporated azo dye derivatives, Arab. J. Chem. 9 (2) (2016) 1643–1648, doi:10.1016/j.arabjc.2012.04.018.

[32] Z. Yu, G. Shi, Q. Sun, H. Jin, Y. Teng, K. Tao, G. Zhou, W. Liu, F. Wen, T. Hou, Design, synthesis and in vitro antibacterial/ antifungal evaluation of novel 1-ethyl-6-fluoro-1, 4-dihydro-4-oxo7 (1-piperazinyl) quinoline-3-carboxylic acid derivatives, Eur. J. Med. Chem. 44 (11) (2009) 4726–4733, doi:10.1016/j.ejmech.2009.05.028.

[33] M. Gaber, Y.S. El-Sayed, K.Y. El-Baradie, R.M. Fahmy, Complex formation, thermal behavior and stability competition between Cu(II) ion and Cu0 nanoparticles with some new azo dyes. Antioxidant and in vitro cytotoxic activity, Spect. Acta Part A: Mol. Biomol. Spect. 107 (2013) 359–370, doi:10.1016/j.saa.2013.01.039.
[34] H.F. Rizk, S.A. Ibrahim, M.A. El-Borai, Synthesis, dyeing performance on polyester fiber and antimicrobial studies of some novel pyrazolotriazine and pyrazolyl pyrazolone azo dyes, Arab. J. Chem. 10 (2) (2017) 3303–3309, doi:10.1016/j.arabjc.2014.01.008.
[35] Z. Sze'kely, P. Fábián, L.L. Torday, C.J. Michejda, A. Aszalós, A. Binding between the CD4 receptor and polysulfonated azo-dyes. An exploratory theoretical study on action-mechanism1, J. Mol. Struc 423 (1–2) (1998) 153–159, doi:10.1016/S0166-1280(97)00363-1.
[36] M. Sirajuddin, S. Ali, V. McKee, H. Ullah, Synthesis, spectroscopic characterization and in vitro antimicrobial, anticancer and antileishmanial activities as well interaction with Salmon sperm DNA of newly synthesized carboxylic acid derivative, 4-(4- methoxy-2-nitrophenylamino)-4-oxobutanoic acid, Spectrochimica Acta Part A: Mol. Biomol. Spec. 138 (2015) 569–578, doi:10.1016/j.saa.2014.11.061.
[37] R.A. Ahmadi, S. Amani, Synthesis, Spectroscopy, Thermal Analysis, Magnetic Properties and Biological Activity Studies of Cu(II) and Co(II) Complexes with Schiff Base Dye Ligands, Molecules 17 (2012) 6434–6448, doi:10.3390/molecules17066434.
[38] A.A. Jarrahpour, A.R. Esmaeilbeig, M. Zarei, Synthesis of 2-hydroxy-3-methoxy-5-(4-methoxyphenylazo) benzaldehyde. A new aldehyde for the preparation of biologically active molecules, Molbank M-37 (2004) 1–2 http://mdpi.org/molbank/molbank2004/m0371.htm1.
[39] V.M. Dembitsky, T.A. Gloriozova, V.V. Poroikov, Pharmacological and Predicted Activities of Natural Azo Compounds, Nat. Prod. Bioprospect. 7 (2017) 151–169, doi:10.1007/s13659-016-0117-3.
[40] T. Tahir, M. Ashfaq, H. Asghar, M.I. Shahzad, R. Tabassum, A. Ashfaq, Medicinal Importance of Azo and Hippuric Acid Derivatives, Mini Rev. Med. Chem. 18 (0) (2018) 1–13, doi:10.2174/1389557518666180727162018.
[41] J.E. Lesch, in: Chapter 3: Prontosil". The first Miracle drugs: How the Sulfa Drugs Transformed Medicine, Oxford University Press, Oxford, 2007, p. 51. Page ISBN 978-0-19-518775-5.
[42] E. Török, E. Moran, F. Cooke, in: Oxford Handbook of Infectious Diseases and Microbiology, Oxford University Press, Oxford, 2009, p. 56. ISBN 9780191039621.
[43] O.P. Gupta, K.K. Agarwal, Role of Phenazopyridine in Urinary Tract Infections, Ind. J. Clin. Pract. 22 (9) (2012) 437–441.
[44] B. Purwono, C. Anwar, A. Hanapi, Syntheses of Azo-Imine derivatives from vanillin as an acid base indicator, Indones. J. Chem. 13 (1) (2013) 1–6, doi:10.22146/ijc.21318.
[45] Y. Hu, S. Hua, F. Li, Y. Jiang, X. Bai, D. Li, N. Li, Green-synthesized gold nanoparticles decorated graphene sheets for label-free electrochemical impedance DNA hybridization, Biosens. Bioelectron 26 (11) (2011) 4355–4361, doi:10.1016/j.bios.2011.04.037.
[46] S. Saha, G. Basak, B. Sinha, Physico-chemical characterization and biological studies of newly synthesized metal complexes of an Ionic liquid-supported Schiff base: 1-{2-[(2-hydroxy-5-bromobenzylidene) amino] ethyl}-3- ethylimidazolium tetrafluoroborate, J. Chem. Sci. 30 (9) (2018) 1–9, doi:10.1007/s12039-017-1409-9.
[47] S. Saha, A. Das, K. Acharjee, B. Sinha, Synthesis, characterization and antibacterial studies of Mn(II) and Co(II) complexes of an ionic liquid tagged Schiff base, J. Serb. Chem. Soc. 81 (10) (2016) 1151–1159, doi:10.2298/JSC160425065S.
[48] R. Huey, G.M. Morris, The Scripps Research Institute, USA, (2008), 54–56.
[49] X.Y. Meng, H.X. Zhang, M. Mezei, M. Cui, Molecular docking: a powerful approach for structure-based drug discovery, Curr. comput-aid drug. 7 (2) (2011) 146–157, doi:10.2174/157340911795677602.
[50] T. Khan, A.J. Lawrence, I. Azad, S. Raza, A.R. Khan, Molecular Docking Simulation with Special Reference to Flexible Docking Approach, JSM Chemistry 6 (1) (2018) 1053–1057.
[51] L.G. Ferreira, R.N. dos Santos, G. Oliva, A.D. Andricopulo, Molecular Docking and Structure-Based Drug Design Strategies, Molecules 20 (2015) 13384–13421, doi:10.3390/molecules200713384.
[52] K. Ohtawara, H. Teramae, Study on optimization of molecular structure using Hamiltonian algorithm, Chem. Phys. Lett. 390 (2004) 84–88, doi:10.1016/j.cplett.2004.03.088.
[53] O. Trott, A.J. Olson, AutoDock Vina: improving the speed and accuracy of docking with a new scoring function, efficient optimization and multithreading, J. Comput. Chem. 31 (2020) 455–461, doi:10.1002/jcc.21334.
[54] W.L. DeLano, Pymol: an open-source molecular graphics tool, CCP4 Newsletter on protein crystallography 40 (1) (2002) 82–92.
[55] G.M. Morris, D.D. Goodsell, R.S. Halliday, R. Huey, W.E. Hart, R.K. Belew, A.J. Olson, Automated docking using a Lamarckian genetic algorithm and an empirical binding free energy function, J. Comput. Chem. 19 (14) (1998) 1639–1662, doi:10.1002/(SICI)1096-987X(19981115)19:14(1639:AID-JCC10)3.0.CO;2-B.
[56] M.A. Alamri, M.T. Ul Qamar, M.U. Mirza, R. Bhadane, S.M. Alqahtani, I. Muneer, M. Froeyen, O.M.H. Salo-Ahen, Pharmacoinformatics and molecular dynamics simulation studies reveal potential covalent and FDA-approved inhibitors of SARS-CoV-2 main protease 3CLpro, J. Biomol. Struct. Dyn (2020) 1–14, doi:10.1080/07391102.2020.1782768.
[57] V.S. Kumar, Y.S. Mary, K. Pradhan, D Brahman, Y.S Mary, R Thomas, M.S Roxy, C Van Alsenoy, Synthesis, spectral properties, chemical descriptors and light harvesting studies of a new bioactive azo imidazole compound, J. Mol. Struct 1199 (2020) 1–10, doi:10.1016/j.molstruc.2019.127035.
[58] B. Li, Y.-Q. Li, Y.-P. Caib, M.Y. Zhou, 1-{2-[(2-*hydroxybenzylidene*)-*amino*]-ethyl}-3-methyl-3H-imidazolium hexafluorophosphate. Structure Reports, ACTA CRYSTALLOGR E. e64 (2008) o2365, doi:10.1107/S1600536808037124.
[59] B. Li, Y.-Q. Li, W.J. Zheng, M.-Y. Zhou, Synthesis of ionic liquid-supported Schiff bases, ARKIVOC, (xi), (2009) 165–171.
[60] B. Khungar, M.S. Rao, K. Pericherla, P. Nehra, N. Jain, J. Panwar, A. Kumar, Synthesis, characterization and microbiocidal studies of novel ionic liquid tagged Schiff bases, CR. CHIM 15 (2012) 669–674, doi:10.1016/j.crci.2012.05.02.
[61] A. Cinarli, D. Gürbüz, A. Tavman, A.S. Birteksöz, Synthesis, spectral characterizations and antimicrobial activity of some schiff bases of 4-chloro-2-aminophenol, B. Chem. Soc. Ethiopia 25 (3) (2011) 407–417, doi:10.4314/bcse.v25i3.68593.
[62] J.E. Kovacic, The C=N stretching frequency in the infrared spectra of Schiff's base complexes—I. Copper complexes of salicylidene anilines, Spectrochim. Acta A Mol. Biomol. Spectrosc. 23 (1) (1967) 183–187, doi:10.1016/0584-8539(67)80219-8.
[63] Y. Wang, R.A. Poirier, Factors That Influence the C=N Stretching Frequency in Imines, J. Phys. Chem. A 101 (5) (1977) 907–912, doi:10.1021/jp9617332.
[64] I.A. Mohammed, A. Mustapha, Synthesis of New Azo Compounds Based on N-(4- Hydroxypheneyl)maleimide and N-(4-Methylpheneyl)maleimide, Molecules 15 (2010) 7498–7508, doi:10.3390/molecules15107498.
[65] J.J. Max, C. Chapados, Infrared Spectroscopy of Aqueous Carboxylic Acids: Comparison between Different Acids and Their Salts, J. Phys. Chem. A 108 (16) (2004) 3324–3337, doi:10.1021/jp036401t.
[66] Y.M. Issa, H.B. Hassib, H.E. Abdelaal, 1H NMR, 13C NMR and mass spectral studies of some Schiff bases derived from 3-amino-1,2,4-triazole Spectrochim, Acta A Mol. Biomol. Spectrosc. 74 (4) (2009) 902–910, doi:10.1016/j.saa.2009.08.042.
[67] S. Hari, In silico molecular docking and ADME/T analysis of plant compounds against IL17A and IL18 targets in gouty arthritis, J. Appl. Pharm. Sci. 9 (7) (2019) 18–26, doi:10.7324/JAPS.2019.90703.
[68] K. Boussery, F.M. Johan, V. De Voorde, Chapter 31 - Physiological Aspects Determining the Pharmacokinetic Properties of Drugs, The Practice of Medicinal Chemistry (2008) 637–654, doi:10.1016/B978-0-12-374194-3.00031-7.
[69] F. Ntie-Kang, L.L. Lifongo, J.A. Mbah, L.C.O. Owono, E. Megnassan, L.M. Mbaze, P.N. Judson, W. Sippl, A.M.N. Efange, In silico drug metabolism and pharmacokinetic profiles of natural products from medicinal plants in the Congo basin, In Silico Pharmacol. 1 (12) (2013) 1–11, doi:10.1186/2193-9616-1-12.
[70] R. Al-Salahi, H.A. Abuelizz, H.A. Ghabbour, R. El-Dib, M. Marzouk, Molecular docking study and antiviral evaluation of 2-thioxo-benzo[g] quinazolin-4(3H)-one derivatives, Chem. Cent. J. 10 (21) (2016) 1–7, doi:10.1186/s13065-016-0168-x.
[71] J. Zhenming, D. Xiaoyu, X. Yechun, D. Yongqiang, L. Meiqin, Z. Yao, Z. Bing, L. Xiaofeng, Z. Leike, P. Chao, D. Yinkai, Y. Jing, W. Lin, Y. Kailin, L. Fengjiang, J. Rendi, Y. Xinglou, Y. Tian, L. Xiaoce, Y. Xiuna, B. Fang, L. Hong, L. Xiang, W.G. Luke, X. Wenqing, X. Gengfu, Q. Chengfeng, S. Zhengli, J. Hualiang, R. Zihe, Y. Haitao, Structure of Mpro from SARS-CoV-2 and discovery of its inhibitors, Nature 582 (2020) 289–293, doi:10.1038/s41586-020-2223-y.
[72] K. Anand, G.J. Palm, J.R. Mesters, S.G. Siddell, J. Ziebuhr, R. Hilgenfeld, (2002). Structure of coronavirus main proteinase reveals combination of a chymotrypsin fold with an extra alpha-helical domain, EMBO J. 21 (13) (2002) 3213–3224, doi:10.1093/emboj/cdf327.
[73] K.S. Chan, S.T. Lai, C.M. Chu, E. Tsui, C.Y. Tam, M.M.L. Wong, M.W. Tse, T.L. Que, J.S.M. Peiris, V.C.W. Wong, K.Y. Yuen, Treatment of severe acute respiratory syndrome with lopinavir/ritonavir: a multicentre retrospective matched cohort study, Hong Kong Med J. 9 (6) (2003) 399–406.
[74] H. Yang, M. Yang, Y. Ding, Y. Liu, Z. Lou, Z. Zhou, L. Sun, L. Mo, S. Ye, H. Pang, G.F. Gao, K. Anand, M. Bartlam, R. Hilgenfeld, Z. Rao, The crystal structures of severe acute respiratory syndrome virus main protease and its complex with an inhibitor, PNAS 100 (23) (2003) 13190–13195, doi:10.1073/pnas.1835675100.
[75] X. Xue, H. Yu, H. Yang, F. Xue, Z. Wu, W. Shen, J. Li, Z. Zhou, Y. Ding, Q. Zhao, X.C. Zhang, M. Liao, M. Bartlam, Z. Rao, Structures of two coronavirus main proteases: implications for substrate binding and antiviral drug design, J. Virol. 82 (5) (2008) 2515–2527 (2008), doi:10.1128/JVI.02114-07.
[76] H. Yang, W. Xie, X. Xue, K. Yang, J. Ma, W. Liang, Q. Zhao, Z. Zhou, D. Pei, J. Ziebuhr, R. Hilgenfeld, K.Y. Yuen, L. Wong, G. Gao, S. Chen, Z. Chen, D. Ma, M. Bartlam, Z. Rao, Design of Wide-Spectrum Inhibitors Targeting Coronavirus Main Proteases, PLoS Biol. 3 (10) (2005) 1–11, doi:10.1371/journal.pbio.0030324.
[77] M.U. Mirza, M. Froeyen, Structural elucidation of SARS-CoV-2 vital proteins: computational methods reveal potential drug candidates against main protease, Nsp12 polymerase and Nsp13 helicase, J. Pharma. Anal. (2020) article in press, doi:10.1016/j.jpha.2020.04.008.
[78] Y. Shimamoto, Y. Hattori, K. Kobayashi, K. Teruya, A. Sanjoh, A. Nakagawa, E. Yamashita, K. Akaj, Fused-ring structure of decahydroisoquinolin as a novel scaffold for SARS 3CL protease inhibitors, Bioorg. & Med. Chem. 23 (4) (2015) 876–890, doi:10.1016/j.bmc.2014.12.028.
[79] M. Wang, R. Cao, L. Zhang, X. Yang, J. Liu, M. Xu, Z. Shi, Z. Hu, W. Zhong, G. Xiao, Remdesivir and chloroquine effectively inhibit the recently emerged novel coronavirus (2019-nCoV) in vitro, Cell Res. 30 (2020) 269–271, doi:10.1038/s41422-020-0282-0.

[80] J. Lim, S. Jeon, H.Y. Shin, M.J. Kim, Y.M. Seong, W.J. Lee, K.W. Choe, Y.M. Kang, B. Lee, S.J. Park, Case of the Index Patient Who Caused Tertiary Transmission of Coronavirus Disease 2019 in Korea: the Application of Lopinavir/Ritonavir for the Treatment of COVID-19 Pneumonia Monitored by Quantitative RT-PCR, J. Kor. Med. Sci. 35 (6) (2020) 1–6 e79, doi:10.3346/jkms.2020.35.e79.

[81] M.L. Holshue, C. DeBolt, S. Lindquist, K.H. Lofy, J. Wiesman, H. Bruce, C. Spitters, K. Ericson, S. Wilkerson, A. Tural, G. Diaz, A. Cohn, L. Fox, A. Patel, S.I. Gerber, L. Kim, S. Tong, X. Lu, S. Lindstrom, M.A. Pallansch, W.C. Weldon, H.M. Biggs, T.M. Uyeki, S.K. Pillai, First Case of 2019 Novel Coronavirus in the United States, New Eng. J. Med. 382 (2020) 929–936, doi:10.1056/NEJMoa2001191.

[82] L.G. Ferreira, R.N. dos Santos, G. Oliva, A.D. Andricopulo, Molecular Docking and Structure-Based Drug Design Strategies, Molecules 20 (2015) 13384–13421, doi:10.3390/molecules200713384.

[83] C.-.W. Lin, Tsai C-H, F.-.J Tsai, P.-.J Chen, C.-.C Lai, L Wan, H.-.H Chiu, K.-.H Lin, Characterization of Trans- and Cis-Cleavage Activity of the SARS Coronavirus 3CLpro Protease: basis for the in Vitro Screening of anti-SARS Drugs, FEBS Lett. 574 (2004) 131–137, doi:10.1016/j.febslet.2004.08.017.